

Cross-sectional analysis of anatomical shape change over time via statistics on 4D within-subject flows

Ali R. Khan¹, Alain Trouvé², and Mirza Faisal Beg¹

¹ School of Engineering Science, Simon Fraser University, 8888 University Drive, Burnaby BC, V5A 1S6, Canada

`akhanf@sfu.ca`, `mfbeg@ensc.sfu.ca`

² CMLA, Ecole Normale Supérieure, 61, Av. du Président Wilson, 94235 Cachan Cédex, France

`trouve@cmla.ens-cachan.fr`

Abstract. Anatomical shape change over time is a biomarker for tracking disease progression. Given a database of anatomical images where each subject is represented by a time-series of images that have been acquired over time, algorithms for estimation of longitudinal progression of morphometric changes over time are required to address 1) the common practical issue where not all subjects are sampled at uniform and homogenous time instants, and 2) the fact that the baseline image for each subject is different hence changes with respect to baseline for each subject are with respect to a different starting frame of reference. To address the first issue, we have previously shown how to estimate the flow of vector fields interpolating through the given time-series of followup images starting from each subject's baseline image in the large deformation diffeomorphic metric matching (LDDMM). In this work, we show one way of addressing issue 2, namely, the normalization of the 4D within-subject flows estimated with respect to individual baseline images into a common central template. We apply this method on the hippocampus shape taken from a small database of 5 controls and 5 cognitively-impaired no dementia (CIND) subjects that underwent magnetic resonance (MR) imaging every 3-6 months over 2 years. The time-series images for each subject were segmented for extracting the hippocampus using an automated multi-atlas segmentation method, and these were used to generate the longitudinal within-subject flow of vector fields with reference to the baseline shape. Then, these flows were transformed into a central unbiased hyper-template shape created from the baseline shapes to provide a common frame of reference. In this central template frame of reference, standard statistical methods can be applied to the 4D vector fields, such as average flows and principle modes of variation in the 4D flows. We computed the means and principal modes of variations for both the control and the CIND group in the central template and demonstrate their time evolution. Statistical analysis on the dimensionality-reduced flow showed significant group differences in the hippocampus shape change over time between the controls and the CIND group. With the increasing availability of time-series data, this method is likely to find use in

understanding the space-time patterns of evolution of anatomical change in normal control subjects and those within a disease group.

1 Introduction

Morphometric quantification of shape change over time is a potentially promising tool for early detection, diagnosis, and followup of diseases that demonstrate distinguishable space-time patterns of progression in the acquired in-vivo images. With the increasing trend towards acquisition of longitudinal datasets containing several 3D anatomical images acquired over time for each individual, techniques for the analysis of shape changes occurring over time have become increasingly desirable. Several databases now exist and are being collected that provide images of human anatomy, in particular, the living human brain in controls and disease taken at several time points for each individual. Cross-sectional analysis of these time-indexed changes is challenging as 1) images are not acquired at the same time-instant for each individual, 2) some individuals may miss some imaging sessions, and 3) although each subject's baseline can serve as his/her own control, relating shape changes over time computed with respect to baseline of the individual subject to changes in others across the database is challenging as each subject's baseline image is different.

The dynamic growth model [1, 2], which constructs deformations of a baseline template image to represent the time series of images acquired over time, presents a natural choice to represent within-subject time-indexed shape change due to its inherent smoothness obtained by parameterizing the deformation in terms of smooth time-indexed velocity vector fields that define the deformations. Extension to interpolating and representing shape evolution in a discrete set of time-indexed images was presented in our previous work [3] allowing the accommodation of irregularly time-sampled or missing data. Only a few techniques now exist to analyze the time-series of images where more than two images are given for each subject. One of these recent techniques is the point-set based time-sequence diffeomorphic metric mapping and a parallel transport mechanism to compare shape change over time across subjects [4]. Another technique, also using point sets, performed longitudinal shape regression along with spatio-temporal pairwise registration to facilitate cross-subject longitudinal comparisons [5]. Previous work in cardiac motion analysis used non-rigid registration of end-diastolic images to compare cross-subject motion fields [6] in a common reference frame, but did not perform quantitative analysis of the motion fields. More recently, mean motion models of respiratory lung motion [7] were generated using the Log-Euclidean mean of mapped transformations obtained via intra-subject and inter-subject diffeomorphic registration.

This paper presents a principled method for the construction and cross-sectional statistical analysis of the flow of velocity vector fields for describing shape change of volumetric 3D brain structures taken from magnetic resonance grayscale images (MRI) acquired over time. The first step is to segment the structure of interest, in this case, the hippocampus, from the time-series of in-vivo

brain images. The segmentation is performed with a standard multi-atlas fusion strategy. Using these binary images representing anatomical shape, the next step is to estimate a within-subject flow carrying the subject’s baseline segmentation image through corresponding segmentations from each of the acquired followup images. To account for heterogeneity in baseline images for comparison across subjects in a database, an unbiased central hyper-template image is computed. The novel contribution of this paper is a method to normalize each within-subject 4D flow to the frame of reference of this central template. This transfer of frame of reference creates a correspondence between different within-subject flows that were each constructed with respect to a different baseline image. Finally, the mean and ‘principal directions’ of time evolution are computed to explore the group differences in the given populations. We test and evaluate our framework on the evolution of hippocampal shape over time in a set of 5 controls and 5 patients (cognitively-impaired no dementia or CIND subjects), each scanned several times over 2 years.

2 Method & Materials

2.1 Automated subcortical segmentation with multi-atlas fusion

Accurate segmentation of MRI images over time within an individual is important as changes due to disease processes can be subtle and easily swamped by errors in segmentation. Automated atlas-based methods for subcortical segmentation, in particular multi-atlas fusion, have been shown to be reasonably accurate [8]. In this approach, several images are designated as database templates, and manually segmented to obtain accurate representations of the object of interest. In the experiments presented here, a group of six brain MRI scans from elderly subjects with manually delineated segmentations were designated as templates. Each of these templates is then used to segment each target brain image in the database resulting in six segmentations for each target brain image, which are then fused to create a final segmentation. This step was conducted using our existing large deformation atlas-based brain MRI segmentation approach [9], which used Freesurfer automated segmentation labels to initialize a region of interest (ROI) for subsequent grayscale image registration. The manual segmentation from each template was propagated using the resulting transformation after grayscale matching to generate the target segmentation, and multiple target segmentations were fused via a simple voxel-based average to create the final target segmentation. Several techniques can be used to generate automated segmentations, and depending on the particular application, some techniques may be more advantageous than others. The final result is a set of 3D segmentations representing the anatomy of interest as observed in each baseline and follow-up image.

2.2 Construction of 4D within-subject flow from discrete image time-series

To represent the change in shape over time with respect to baseline, a smooth velocity vector field v_t^k that evolves the baseline ($t = 0$) image I_0^k for subject k to interpolate through the given time-indexed samples $I_{t_j=0\dots N}^k$ is computed. This flow is estimated via the basic variational problem in the space of smooth velocity vector fields V on domain Ω by minimizing the energy functional:

$$E(v) = \int_0^T \|v_t^k\|_V^2 dt + \lambda \sum_{j=1}^N \|I_{t_0}^k \circ \phi_{t_j,0}^k - I_{t_j}^k\|_{L^2}^2.$$

This equation is solved via a gradient descent approach described in [3]. The mappings $\phi_t^k = \phi_{0,t}^k$ are also found via semi-lagrangian integration of the flow, so that $I_t^k \approx \phi_{0,t}^k \cdot I_0^k = I_0^k((\phi_t^k)^{-1}) = I_0^k(\phi_{t,0}^k)$. Note that time $t = [0, T]$, is related to the physical time between followup images, enabling the energy function to deal with irregular temporal sampling of followup images or missing data.

2.3 Normalization of 4D within-subject flow to a central template

A single central hyper-template I^* is generated based on a group-wise average estimation of all baseline image segmentations [10]. Each subject's baseline image I_0^k is then spatially normalized to this template such that $I_0^k \approx \phi_{\star,0}^k \cdot I^* = I^*(\phi_{0,\star}^k)$. Finally, each within-subject flow is normalized to the template by transforming the flow from each time instant t using the composition of mappings from $t \mapsto 0 \mapsto \star$. The maps $\phi_{\star,t}^k = \phi_{0,t}^k \circ \phi_{\star,0}^k$ and $\phi_{t,\star}^k = \phi_{0,\star}^k \circ \phi_{t,0}^k$ refer to transfer of coordinates between the hyper-template and each time instant along the flow for the k -th subject. Define the Ad operator as

$$Ad_\psi(v) = D\psi \circ \psi^{-1} v \circ \psi^{-1},$$

which describes the transformation of vector data, v , with the map, ψ , taking into account the Jacobian change of variables at each grid point in v . The transfer of the within-subject 4D flow, $v^k = (v_t^k), t \in [0, T]$, into the coordinates of the template I^* is accomplished via

$$w_t^k = Ad_{\phi_{\star,t}^k} v_t^k = D\phi_{\star,t}^k \circ \phi_{\star,t}^k v_t^k \circ \phi_{\star,t}^k \quad (1)$$

In this equation, for each Eulerian grid-point x in the template I^* , the point $\phi_{\star,t}^k(x)$ is the mapping of this point to the corresponding point in the flow at time t . The velocity at that point $v_t^k(\phi_{\star,t}^k(x))$ is found by interpolation from surrounding Eulerian grid-points. Then, this velocity vector is mapped back to the template via the Jacobian of the map $D\phi_{\star,t}^k$ computed at the point $\phi_{\star,t}^k(x)$ ie $D\phi_{\star,t}^k(\phi_{\star,t}^k(x))$. One way to compute $D\phi_{\star,t}^k(\phi_{\star,t}^k(x))$ is by using interpolation from the Jacobian values calculated at the neighboring Eulerian grid points. Alternatively, since $v_t^k(\phi_{\star,t}^k(x)) = D\phi_{\star,t}^k(x)w_t^k(x)$, then $w_t^k(x)$ can be

computed via solving a linear system at each point x . The partial derivatives $\eta_1 = \partial/\partial_{x_1}(\phi_{\star,t})$, $\eta_2 = \partial/\partial_{x_2}(\phi_{\star,t})$, $\eta_3 = \partial/\partial_{x_3}(\phi_{\star,t})$ are available at each point x , and the velocity $v_t^k(\phi_{\star,t}^k(x)) = (b_1 \ b_2 \ b_3)^t$ is available for the point $\phi_{\star,t}^k(x)$. Then, $v_t^k(\phi_{\star,t}^k(x)) = D\phi_{\star,t}^k(x)w_t^k(x)$ where $w_t^k = (a_1 \ a_2 \ a_3)^t$ can be written as $(b_1 \ b_2 \ b_3)^t = a_1\eta_1 + a_2\eta_2 + a_3\eta_3$ and solved using standard techniques.

The procedure specified by Equation 1 maps all within-subject 4D flows to the same central hyper-template removing the individual baseline differences from which the flows were built, and temporally compressing all the 4D vector fields into the coordinates of the hyper-template. Figure 1 shows a visual representation of how 4D within-subject flows are normalized to a central template.

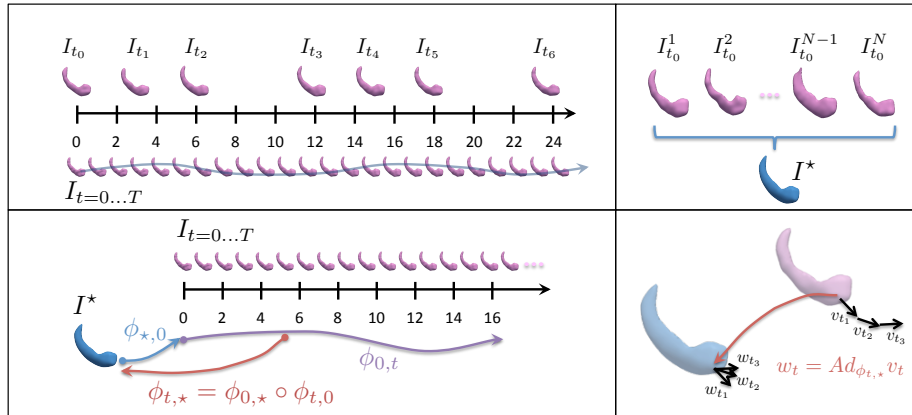


Fig. 1. A schematic showing normalization of a 4D within-subject flow, starting with the generation of the within-subject flows (upper-left), the generation of the hyper-template (upper-right), the composition of the maps from 4D flow to hyper-template (lower-left), and the normalization of the flow into the frame of reference of the central template via the Ad operator (lower-right).

Taking advantage of the vector-space properties of trajectories w_t^k in a common hyper-template, operations such as average flow $\bar{w}_t = (1/M) \sum_{k=1}^M w_t^k$ in the hyper-template can be performed. The average evolution can be defined to be $\bar{\phi}_t$, $\bar{\phi}_0 = \text{id}$ and follows the evolution specified by $d/dt \bar{\phi}_t = D\bar{\phi}_t \bar{w}_t$. The cross-sectional average shape evolution over time is thus given by $\bar{I}_t = \bar{\phi}_t I^* = I^*(\bar{\phi}_t^{-1})$ and also, the Eulerian velocity \bar{v}_t corresponding to the average hyper-template velocity \bar{w}_t is found by $\bar{v}_t = Ad_{\bar{\phi}_t} \bar{w}_t$. The inverse maps $\bar{\phi}_t^{-1} = \phi_{t,0}$ follow the equation

$$\partial/\partial t (\phi_{t,0} \circ \phi_{0,t}) = \partial/\partial t \phi_{t,0}(\phi_{0,t}) + D\phi_{t,0}(\phi_{0,t})D\phi_{0,t}w_t = 0$$

and therefore, $\partial/\partial t \phi_{t,0} = -w_t(\phi_{t,0})$. For the average inverse map, denoting $\bar{\phi}_t^{-1} = \bar{\phi}_{t,0} = \eta_t$, $\bar{\phi}_0^{-1} = \eta_0 = \text{id}$, the equation for the average inverse map

evolution becomes $d/dt \eta_t = -\bar{w}_t(\eta_t)$ which is in the form of the standard ODE $\dot{\phi}_t = v_t(\phi_t)$ implemented previously in [11].

2.4 Statistical evolution of within-subject 4D flows in the hyper-template

By placing each within-subject’s hyper-template normalized flow in a matrix $W = [\mathbf{w}^1 \mathbf{w}^2 \dots \mathbf{w}^M]$ of dimensionality $(n = N_x \times N_y \times N_z \times T \times 3) \times M$, we can perform PCA on this database matrix to find principal components that best capture the variability of the database. By projecting each column of W on the subspace spanned by a reduced set of principal components, we can represent a within-subject 4D flow in the reduced dimensionality space, where the coefficients are directly amenable to statistical tests on the reduced data.

Furthermore, we can also reconstruct the within-subject flows based on a single principal component ‘direction’. Let \hat{W}^{PC_i} be the database matrix formed from the projection of each hyper-template-indexed within-subject flow on the subspace of the i^{th} principal component. The mean over a subset of columns, representing the two groups, would generate the mean trajectory of that subset of subjects along the i^{th} principal component. These hyper-template-indexed ‘principal component flows’ can then be integrated as described above to generate time-evolutions of the hyper-template along those ‘directions’.

2.5 Materials

We applied this proposed methodology on a small pilot dataset of 10 subjects from a study of cognitive-impairment with no dementia (CIND) [12], consisting of 5 CIND and 5 controls, aged 69.9 ± 7.9 years of which 6 were female and 4 were male. Subjects were followed for a period of two years, with MRI (T1 SPGR, 1.5T) scans 3-6 months apart, with six subjects scanned 9 times, one subject scanned 8 times, and three subjects scanned 7 times. Automatic left and right hippocampus segmentations were generated for each MRI using a typical multi-atlas segmentation procedure. All further processing was done separately for the left and right hippocampus. Each subject’s earliest scan was used as the baseline image, with the last followup scan taken 24 months later. Within-subject 4D splines were computed on the left and right hippocampus segmentations separately with $T = 48$ time-steps, corresponding to 24 time-steps per year. This temporal-resolution was chosen considering the trade-off in computational and model complexity with the ability to represent sufficient longitudinal deformation. This is a small database and hence the purpose of this experiment is mainly to demonstrate the feasibility of the technique and not to generalize the results to the control vs CIND groups from which this data was taken.

3 Results

Figure 2 shows the mean template evolution for the control and patient (CIND) groups, at time from baseline of 6, 12, 18, and 24 months. Visualizations of the

evolved template shape at each point of the flow, $t = T$, were generated using an isosurface of the propagated template, colored by the determinant of the Jacobian of the map. PCA was performed on the hyper-template indexed flows to generate reconstructions using each of the 9 principal components, $\hat{W}^{PC_i}, i = 1 \dots 9$. As described earlier, the columns corresponding to flows of the control and CIND subjects were extracted from the database matrix to generate flows along each principal component ‘direction’. The evolved hyper-template shape at the endpoints of these flows are shown in Figure 3 where there are noticeable differences in the evolution of the hyper-template along the principal directions specified by the two groups. For example, the evolution along the left fifth principal component displays a different pattern of atrophy between the controls and the CIND group.

Statistics on mean coefficients along each principal component (the ‘dimensionality-reduced flows’) for each group are plotted in Figure 4. Comparing these plots to the visualizations of Figure 3, one can see the space-time representation of the between-group differences. To determine if there are any statistically significant group differences, we performed two-sided Student t -tests on coefficients along each of the ‘principal directions’, with a null-hypothesis of equal means. We found statistically significant group differences for the left hippocampus’ 5th coefficient (p -value=0.042) and the right hippocampus’ 4th coefficient (p -value=0.0074), all other p -values were higher than 0.05 and are thus not reported.

The top 4 most significant t -test coefficients from each side, (right=[2, 4, 6, 9], left=[2, 5, 6, 9]), were selected to determine if a subset of coefficients along principal components taken together can provide evidence of statistically significant group differences. The Hotelling T^2 statistic was used with permutation testing ($n=10,000$) to determine significance, resulting in significant group differences for both left ($T^2=118.44$, effect size=6.88, p -value=0.0104) and right ($T^2=176.95$, effect size=8.41, p -value=0.0060) hippocampal shape evolution over time.

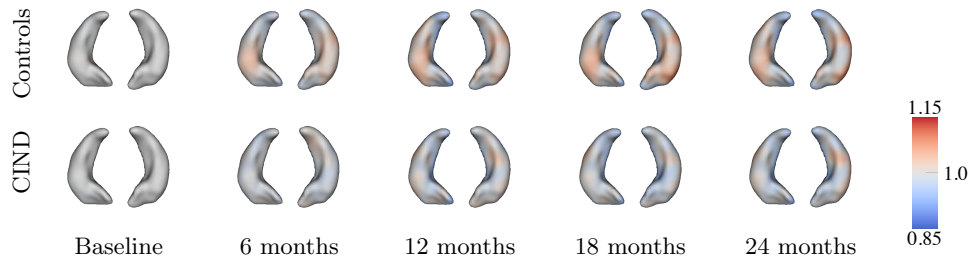


Fig. 2. Mean template time-evolutions for the controls and CIND subsets at times $t = 0, 11, 23, 35, 47$, corresponding to 0, 6, 12, 18, and 24 months, shown coloured with $|D(\bar{\phi}_{0,T})|$ to show volumetric contraction (cool) and expansion (warm). In hippocampal contraction representing atrophy, is observed to be more prevalent in the CIND group in line with the expected pattern of atrophy.

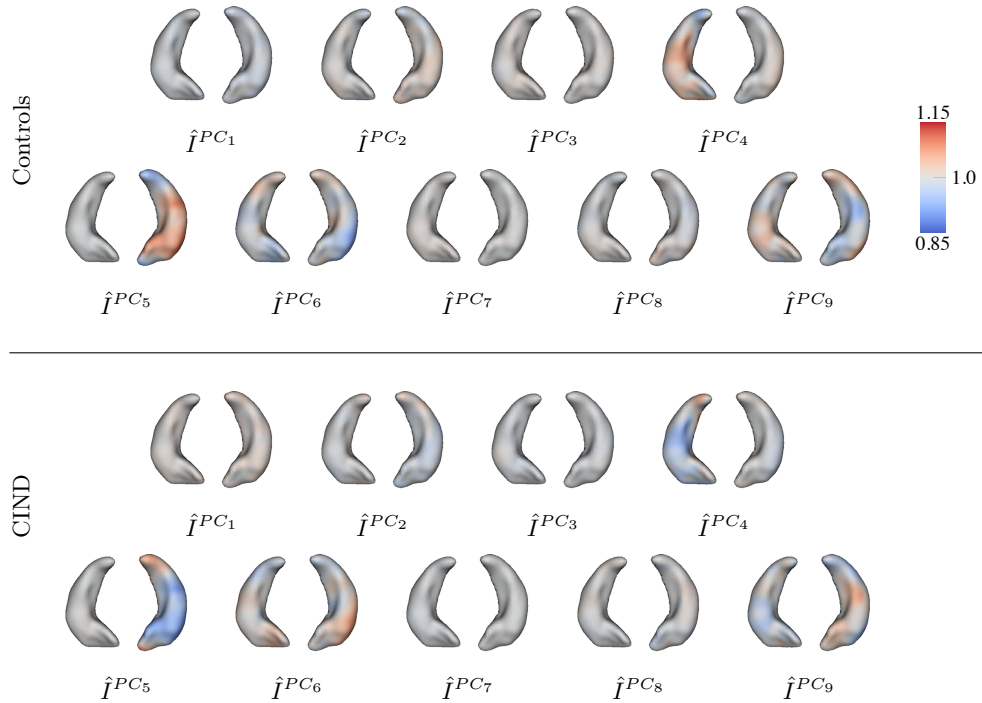


Fig. 3. Modes of variation of controls and CIND within-subject 4D flows in the hyper-template obtained from projections of the individual flows into subspace of single principal components of the database matrix and evolution of the average hyper-template indexed flow (w) to mapping at final time $t = T$, shown coloured with $|D(\phi_{0,T})|$. The color pattern (volumetric contraction (cool) and expansion (warm)) on the hyper-template for the two groups shows differences in some principal components. These results are mainly illustrative of the method as due to the small size of the database used in this experiment, their generalization is limited.

4 Conclusions & Discussion

Construction of hyper-template normalized within-subject 4D shape representations using volumetric images acquired over time is likely to be an important tool for discovering and comparing the space-time progression of various neuro-degenerative diseases. In this paper, we show one method that uses multi-atlas segmentation of each time-series MR image to construct the within-subject flows, followed by transforming them to a single central hyper-template. This template-normalized 4D flow can then be subjected to statistical analysis to discover modes of variation in the database, and visualize the evolution of the hyper-template along these modes of variation.

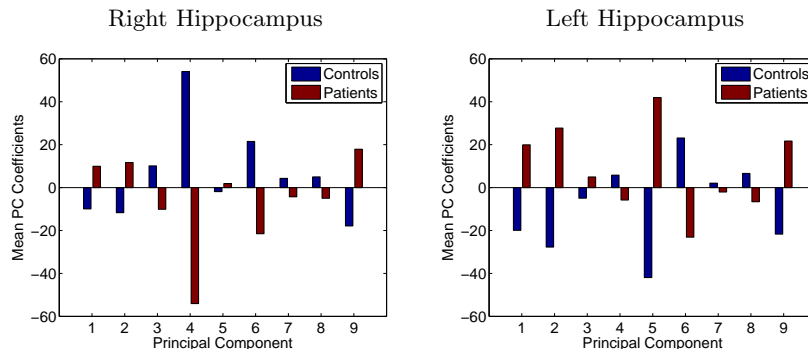


Fig. 4. The bar plots show the mean coefficients from the control and CIND groups for each PC calculated from the database matrix. The average projections of the controls group and the CIND group along the ‘principal modes’ show distinguishing features that may be representative of the underlying differences in disease state.

The Ad-operator based approach presented here offers some methodological advantages. In contrast to the method of parallel transport that relies on a geodesic path of transformation between individual baseline shapes and central hyper-template to create an isometry between tangent spaces and is thus path dependent, our proposed Ad-operator approach of transforming flows does not depend on the path and corresponds only to a change of reference frame. Therefore, our approach can be used with any transformation between the hyper-template and the baseline shapes, and does not require a geodesic shortest path transformation. The normalization by the Jacobian of the transformation in this Ad-operator approach as seen in Equation 1 also has mathematically desirable properties in handling issues of scaling across varying anatomical sizes across subject’s baseline shapes. Baseline neuroanatomical shapes of different subjects may be of varying sizes reflecting different cranial vault size. Longitudinal morphometric changes with respect to a smaller (with respect to the hyper-template) baseline shape are scaled up versus changes seen in relation to a larger (with respect to hyper-template) baseline shape. The issue of size, and how to compare changes that are with respect to different ‘size’ baselines is an important issue in longitudinal analysis, and this formulation gives one way of incorporating scaling of measurements in the analysis.

The experiments presented in this work are on a small database limited due to our data sharing agreement and hence mainly for demonstration of the method; particular observations regarding patterns of atrophy seen in this experiment will require further confirmation on a larger database. Visualization of shape evolutions of controls vs CIND along the database principal components (the ‘modes’ of shape evolution) demonstrate several distinguishing features such as prevalence of regions of inward deformations in CIND group. These differences are indicative that this method could potentially be a useful tool to discover the

modes of progression of of morphometric shape change over time given a larger database.

Another important issue not addressed here before valid longitudinal comparisons can be made across the database is the considerable heterogeneity in the baseline image with respect to placement in time along the disease process. Although individuals in the database are grouped in overarching categories such as controls and CIND, they are likely in different phases of the disease evolution, and the disease may also be evolving at differing rates within individuals. Thus, choosing a baseline image that represents the same stage in the disease across individuals is an important consideration to compare shape evolutions over similar time-course of the disease, as well as some form of time matching to account for the heterogeneity in the speed of evolution of the disease. These issues are not straightforward to address as most imaging databases are acquired over a fixed duration in time with limited imaging samples. For our experiments thus, the first available scan of each individual was chosen as their ‘baseline’ even though these baseline states represent different states for each individual. Given a longer study duration, a better choice would be to temporally align the longitudinal time-sequences according to some measurable event, such as disease onset but due to limited imaging samples, and small numbers of subjects, this may not always be feasible.

In conclusion, this paper presents a method for the normalization of 4D within-subject flows of vector fields constructed with respect to individual subject baseline shapes into the frame of reference of a single central hyper-template shape. This provides a way for the cross-sectional analysis of 4D longitudinal flows that can be used to statistically and visually investigate shape changes over time across subjects. This method was demonstrated on a small set of longitudinal MR image database. Although the small size of the database precludes generalization of observations, and the utility is mainly in showing the feasibility of the method, statistically significant group differences between normal controls and cognitively-impaired patients with no dementia were found in testing for group differences in the dimensionality reduced coefficients along the database principal components. Future plans involve application of this methodology to a larger longitudinal dataset and exploration of the time evolution of a larger number of brain structures.

References

1. Miller, M.I., Trounev, A., Younes, L.: On the metrics and Euler-Lagrange equations of computational anatomy. *Annu. Rev. Biomed. Eng.* **4** (2002) 375–405
2. Miller, M.I.: Computational anatomy: shape, growth, and atrophy comparison via diffeomorphisms. *Neuroimage* **23 Suppl 1** (2004) S19–33
3. Khan, A., Beg, M.: Representation of time-varying shapes in the large deformation diffeomorphic framework. *IEEE International Symposium on Biomedical Imaging – ISBI 2008* (2008) 1521–1524
4. Qiu, A., Albert, M., Younes, L., Miller, M.I.: Time sequence diffeomorphic metric mapping and parallel transport track time-dependent shape changes. *Neuroimage* **45**(1 Suppl) (2009) S51–60

5. Durrleman, S., Pennec, X., Trouvé, A., Gerig, G., Ayache, N.: Spatiotemporal atlas estimation for developmental delay detection in longitudinal datasets. *Medical Image Computing and Computer-Assisted Intervention – MICCAI 2009 LNCS* **5761** (2009) 297–304
6. Rao, A., Sanchez-Ortiz, G.I., Chandashekar, R., Lorenzo-Valdes, M., Mohiaddin, R., Rueckert, D.: Comparison of cardiac motion across subjects using non-rigid registration. *MICCAI 2002, LNCS* **2488** (2002) 722–729
7. Ehrhardt, J., Werner, R., Schmidt-Richberg, A., Handels, H.: Prediction of Respiratory Motion Using A Statistical 4D Mean Motion Model. *Proceedings of the Second International Workshop on Pulmonary Image Analysis* (2009) 1–12
8. Heckemann, R., Hajnal, J.V., Aljabar, P., Rueckert, D., Hammers, A.: Automatic anatomical brain MRI segmentation combining label propagation and decision fusion. *Neuroimage* **33**(1) (2006) 115–126
9. Khan, A.R., Wang, L., Beg, M.F.: Freesurfer-initiated fully-automated subcortical brain segmentation in MRI using large deformation diffeomorphic metric mapping. *Neuroimage* **41**(3) (2008) 735–46
10. Joshi, S., Davis, B., Jomier, M., Gerig, G.: Unbiased diffeomorphic atlas construction for computational anatomy. *Neuroimage* **23 Suppl 1** (2004) S151–60
11. Beg, M.F., Miller, M.I., Trouvé, A., Younes, L.: Computing large deformation metric mappings via geodesic flows of diffeomorphisms. *International Journal of Computer Vision* **61**(2) (2005) 139–157
12. Jacova, C., Peters, K.R., Beattie, B.L., Wong, E., Riddehough, A., Foti, D., Scheltens, P., Li, D.K.B., Feldman, H.H.: Cognitive impairment no dementia – neuropsychological and neuroimaging characterization of an amnesic subgroup. *Dement. Geriatr. Cogn. Disord.* **25**(3) (2008) 238–47